Computerized Medical Imaging and Graphics 34 (2010) 651–658

Contents lists available at ScienceDirect

Computerized Medical Imaging and Graphics

journal homepage: www.elsevier.com/locate/compmedimag

Curvature-dependent surface visualization of vascular structures

Jianhuang Wu[a,b,*], Renhui Ma[a,1], Xin Ma[a,2], Fucang Jia[a,3], Qingmao Hu[a,b,4]

[a] Shenzhen Institutes of Advanced Technology, Chinese Academy of Sciences, 1068 Xueyuan Boulevard, University Town of Shenzhen, Xili Nanshan 518055, Shenzhen, China
[b] The Chinese University of Hong Kong, Hong Kong SAR, China

ARTICLE INFO

Article history:
Received 29 September 2009
Received in revised form 24 July 2010
Accepted 30 July 2010

Keywords:
Vessel visualization
Centerline
Bidirectional sampling
Curvature-dependent subdivision

ABSTRACT

Efficient visualization of vascular structures is essential for therapy planning and medical education. Existing techniques achieve high-quality visualization of vascular surfaces at the cost of low rendering speed and large size of resulting surface. In this paper, we present an approach for visualizing vascular structures by exploiting the local curvature information of a given surface. To handle complex topology of loop and multiple parents and/or multiple children, bidirectional adaptive sampling and modified normal calculations at joints are proposed. The proposed method has been applied to cerebral vascular trees, liver vessel trees, and aortic vessel trees. The experimental results show that it can obtain a high-quality surface visualization with fewer polygons in the approximation.

1. Introduction

Three-dimensional (3D) visualization of vascular structures can provide straightforward information of the morphology of vessels, spatial relations among these vessels and other relevant anatomic structures, intuitive depiction of curvature, and depth relations. Thus it can help surgeons to better understand the branching pattern and complex topology of vascular structures for better and quick decision making during surgery and is of vital importance in therapy planning and medical education.

The vascular structures can be visualized by volume rendering or surface rendering. In surface rendering, there are two kinds of methods [1]: model-based and model-free. The former assumes that the cross-section of vessels is circular, while the latter makes no shape assumption of vessel cross-section. Model-based surface visualization methods require centerline extraction and radius estimation from segmented vessels [2–4]. Based on the centerline tree, geometric primitives such as cylinders [5] and truncated cones [6] are used to generate vessel surface for visualization. These model-based methods suffer from the low quality of the reconstruction surface and coarse transitions at vessel branching. To overcome the drawbacks, B-Spline surfaces [7], simplex meshes [8], convolution surfaces [9,10], and subdivision surfaces [11,12] are explored.

The most common model-free technique is Marching Cubes (MC) [13]. Unfortunately, MC has two major limitations: the generated surface depends highly on the chosen isovalue and a slight change in value may result in great change in geometric and even topological features of the produced surface, and the visual quality may be very low because the yielded surface may have aliasing artifacts inappropriate for computational fluid dynamics simulations. Recently, Schumann [14,15] presented a model-free technique which can produce high-quality surface from segmented vessels. The technique, which was originally proposed to reconstruct surface from 3D point cloud, is based on multi-level partition unity implicits [16].

Although the above-mentioned methods like subdivision surface and convolution surface can generate smooth surface, the rendering speed is slow especially when the size of the reconstructed surface is large. Let us take subdivision surface based method, the most advanced technique of model-based visualization of vascular structures [17], for example. Felkel et al. [12] applied Catmull–Clark scheme to the initial mesh for the subdivision surface, which is defined as the limit of a sequence of successive refinements [18]. Unfortunately, the number of polygons grows exponentially with the iteration of subdivision, e.g. an initial vessel surface with 7834 triangles can reach 2,005,504 triangles after only four iterations (each iteration will yield a 3 times increase in polygon). Such a huge number of polygons will not only affect the rendering speed but the post processing, e.g. collision detection as well as real-time vessel deformation simulation.

To achieve a better balance among vascular structure visualization, size of the reconstructed surface, and the rendering speed, this paper presents an approach of curvature-dependent surface visualization of vascular structure. The goal is to obtain a high-quality topologically preserved two-manifold surface with as few polygons

* Corresponding author. Tel.: +86 755 86392115; fax: +86 755 86392194.
E-mail addresses: jh.wu@siat.ac.cn, jianhuang.wu@gmail.com (J. Wu), ma_renhui@yahoo.com.cn (R. Ma), xin.ma@siat.ac.cn (X. Ma), fc.jia@sub.siat.ac.cn (F. Jia), qm.hu@siat.ac.cn (Q. Hu).
[1] Tel.: +86 755 86392120; fax: +86 755 86392194.
[2] Tel.: +86 755 86392060; fax: +86 755 86392299.
[3] Tel.: +86 755 86392116; fax: +86 755 86392194.
[4] Tel.: +86 755 86392117; fax: +86 755 86392194.

0895-6111/$ – see front matter © 2010 Elsevier Ltd. All rights reserved.
doi:10.1016/j.compmedimag.2010.07.006

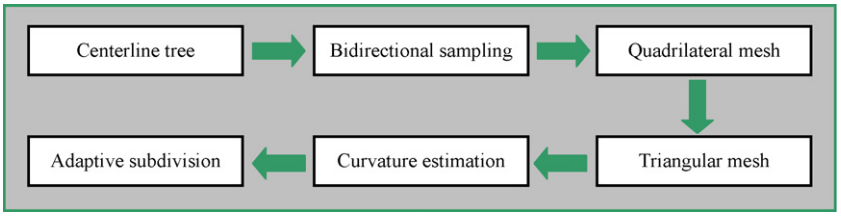

Fig. 1. Flow chart of curvature-dependent visualization of vascular structures.

as possible. To handle complex topology of loop and multiple parents and/or multiple children, bidirectional adaptive sampling and modified normal calculations at joints are proposed.

This paper is organized as follows. Details of the method are described in Section 2. Results and discussion are given in Section 3. Finally, concluding remarks are presented in Section 4.

2. Methodology

The schematic flow chart of the proposed method is illustrated in Fig. 1. The centerline tree from segmented vessels is sampled by the proposed bidirectional sampling technique to improve the surface quality at joints with branches. Then, the quadrilateral mesh is tiled through a recursive branching-construction procedure as described in [11,19] and is converted to triangular mesh. The curvatures of the triangular mesh are estimated for adaptive subdivision.

Though our method bears resemblance to existing method described in [11,19], there are three major differences: (1) the proposed bidirectional sampling versus existing unidirectional sampling, (2) determination of *up-vector* and normal at joint to handle vessels with complex topology in tiling the base quadrilateral mesh, and (3) the proposed adaptive subdivision versus existing uniform subdivision.

2.1. Centerline tree

The input to reconstruct adaptive subdivision surface is vessel centerline tree [11] which is obtained from segmented vessels. The tree (Fig. 2) consists of root (vessel start), joint (vessel branching), parent segment and children segments. Each vessel cross-section is defined by a center vertex with an estimated radius. The center vertices of the cross-sections lie on the centerline and the cross-sections are perpendicular to the centerline. In Fig. 2, the vessel segment *X* is the parent segment of vessel segments *Y* and *Z*. In a centerline tree, a child segment may have multiple parents when the vessel tree has a loop.

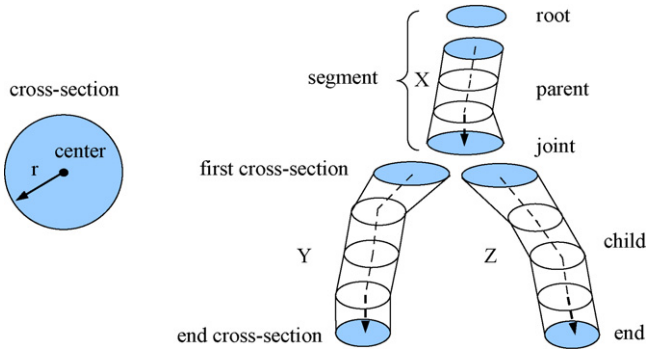

Fig. 2. Vessel centerline tree and its representation (left is the geometry of vessel cross-section and right is vessel tree geometry and segments).

2.2. Bidirectional sampling

To avoid generating a non-manifold initial base mesh, the centerline tree needs to be down-sampled. We propose bidirectional sampling to sample the centerline. The technique samples the centerline from both the first and last vessel cross-section simultaneously using Eq. (1) [19] with the first and last vessel cross-section being kept:

$$x_{i+1} - x_i = g(y_{i+1}) + g(y_i) \quad i \in [0, N-1] \tag{1}$$

where $g(y_i) = \alpha r_i/(1+\beta\kappa_i)$, x_i is the center of the cross-section, r_i and κ_i are the corresponding radius and Gaussian curvature respectively. Generally, α is a positive scalar value, κ_i is obtained according to the way described in [20] and β is a positive weight on curvature influence.

Take the vessel segment illustrated in Fig. 3 for example, the proposed bidirectional sampling procedure works in this way: suppose that the sampling is currently from left to right and the x_i has been kept to check if x_{i+1} should be kept. If the Euclidean distances meet $d(x_{i+1}, x_i) \geq g(y_{i+1}) + g(y_i)$, vertex x_{i+1} is kept; otherwise, the smallest j with x_{i+j} satisfying $d(x_{i+j}, x_i) \geq g(y_{i+j}) + g(y_i)$ ($j \geq 2$) is found, and the average of x_{i+j} and x_{i+j-1} will be taken as the next new vertex. Similarly, the sampling procedure proceeds simultaneously from right to left and stops when they meet at the same sample point. If they do not meet at the same sample point, we check the distance between them. If the distance satisfies $d(x_l, x_r) \leq g(y_l) + g(y_r)$, where x_l (x_r) is the second last sampling point from left to right (right to left), the procedure ends. Otherwise, the average of x_l and x_r is taken as the last sampling point, while the procedure ends.

2.3. Base quadrilateral mesh generation

Once the centerline has been down-sampled, a base mesh is generated with quadrilateral patch along the centerline by a recursive procedure. For the completeness of the paper, we briefly introduce the main procedure. More details can be found from Refs. [11,12,21]. The procedure consists of two parts:

(1) Preprocessing steps, including computation of the directions and normals of segments, classification of segments to forward or backward, joining of normals at branches and determination of *up-vectors*.
(2) Tiling the vessel tree. This part generates the base mesh recursively according to the tree structure (i.e. branching and

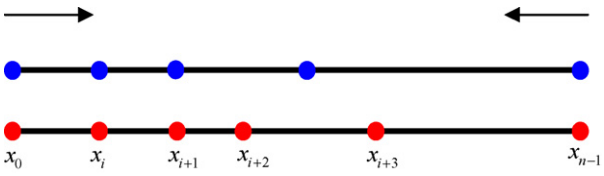

Fig. 3. Bidirectional sampling example (bottom is the centerline to be sampled and top is the sampled result).

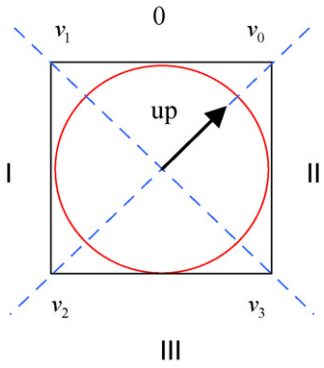

Fig. 4. Definition of *up-vector* (v_0 is in the direction of the *up-vector* which defines the four quadrants in the circular cross-section).

non-branching) for a given level of the tree. For the non-branching vessel tree, the surface is tiled from the second cross-section to the second last cross-section, based on the assumption that the first cross-section has been handled. For the branching part, the surface region is generated by patching the end cross-section and the first cross-sections of the other branches which share the joint.

2.3.1. Determination of up-vector and normals at joints

Determination of normals at joints and *up-vectors* is of paramount importance during tiling of the base mesh, because incorrect *up-vectors* will result in a twisted surface [11], particularly at the joint of branchings. *Up-vector* is defined as the first of the four vectors which equally dissect the square-shape cross-section (Fig. 4) and is propagated along the segments. When dealing with complex topology of vascular structures (e.g. a branch has multiple parents or multiple children), we propose a simple method to calculate the normal vector at the joint as the average of normal vectors of the last cross-section of all incoming parent segments, and the normal vectors of the last cross-sections of these parent branches are replaced by the computed normal vector at the joint. Then, the *up-vector* is projected to the normal plane (defined by the normal and center of the cross-section) along the trunk branch. For other cases such as a branch with only one parent or one child, the normal vector at joint and the *up-vector* are handled as described in [11].

2.4. Curvature estimation

Before estimating the curvature of each vertex, the generated quadrilateral meshes are converted to triangular meshes by bisecting the diagonal of every quad, because we use Loop subdivision scheme [18] which is a face-split scheme for triangular meshes to construct the vessel surface. There are many references about curvature estimation on triangular meshes [22]. In this work, we use a polynomial fitting method which fits a 2-ring neighborhood around a vertex, as this method has a good performance on accuracy and is robust to noise [22]. The 2-ring neighborhood is constructed from the 1-ring (the star of a vertex) by adding all of the vertices of any face containing a vertex of the 1-ring neighborhood. Generally, the polynomial is a second-order polynomial with six coefficients in each coordinate direction.

2.5. Adaptive subdivision

Subdivision surfaces have been widely used in the field of computer graphics as it is easy to generate a smooth surface from arbitrary topology of complex geometric models without trimming/patching, and to deal with multi-resolution analysis of

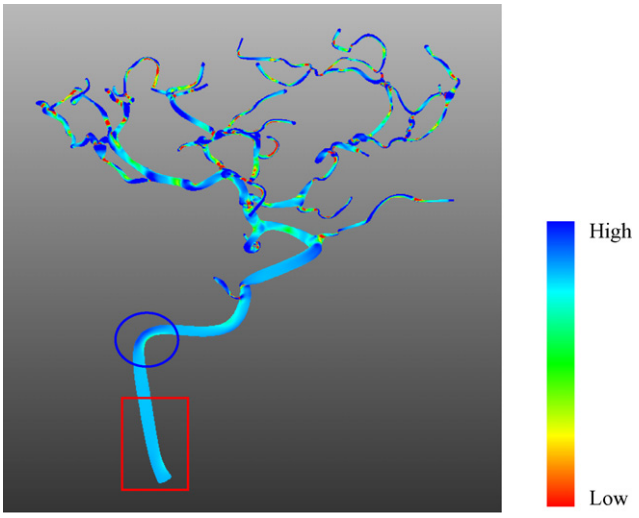

Fig. 5. Color-coded visualization of Gaussian curvature (circle region with high curvature and rectangle region with low curvature).

complex geometry [18]. Therefore, vessel surfaces reconstructed by subdivision surface can be easily tuned to multi-scale visualization and other applications.

In surface sampling and mesh generation, there is a principle that highly curved regions should be densely sampled [23] or triangulated [24] and vice versa. Therefore, to derive a subdivision surface, there is no need to refine the whole model, instead, only areas with high curvature (e.g. blue encircled region shown in Fig. 5) need to be subdivided. In addition, refining a relatively flat surface (e.g. red rectangular region shown in Fig. 5) still generates a flat surface without improving the surface quality. We thus propose to subdivide the generated base mesh depending on curvature to obtain the smooth vessel surface in four steps:

(1) If the converted triangular mesh is coarse, it is subdivided by one level of uniform refinement to attain a reasonable resolution in order to estimate curvature more accurately.
(2) Estimate the curvature for each vertex and the curvatures are processed by histogram equalization after scaling the curvature ranging between 0 and 1.
(3) For every triangle, if the curvatures of all its three vertices lie below a user-specified threshold θ, then this triangle is tagged and will not be subdivided at the next level of subdivision.
(4) Remove cracks [25]. During a subdivision process, if a triangle is to be subdivided but its neighboring triangles are not to be subdivided, a crack is generated which should be removed. A triangle with one neighboring triangle to be subdivided will be split into two triangles (Fig. 6 (left)). For a triangle with two neighboring subdivided triangles, it will be split by two triangle edges (Fig. 6 (middle)). When the triangle has three neighbors to be subdivided, it will be subdivided with regular refinement (Fig. 6 (right)).

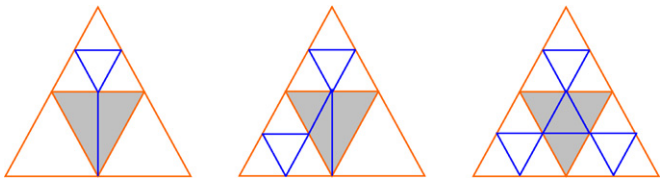

Fig. 6. From left to right, cases of subdivided triangle (grey color) with one, two, and three subdivided neighbors and the corresponding subdivision refinement (blue color). (For interpretation of the references to color in this figure legend, the reader is referred to the web version of the article.)

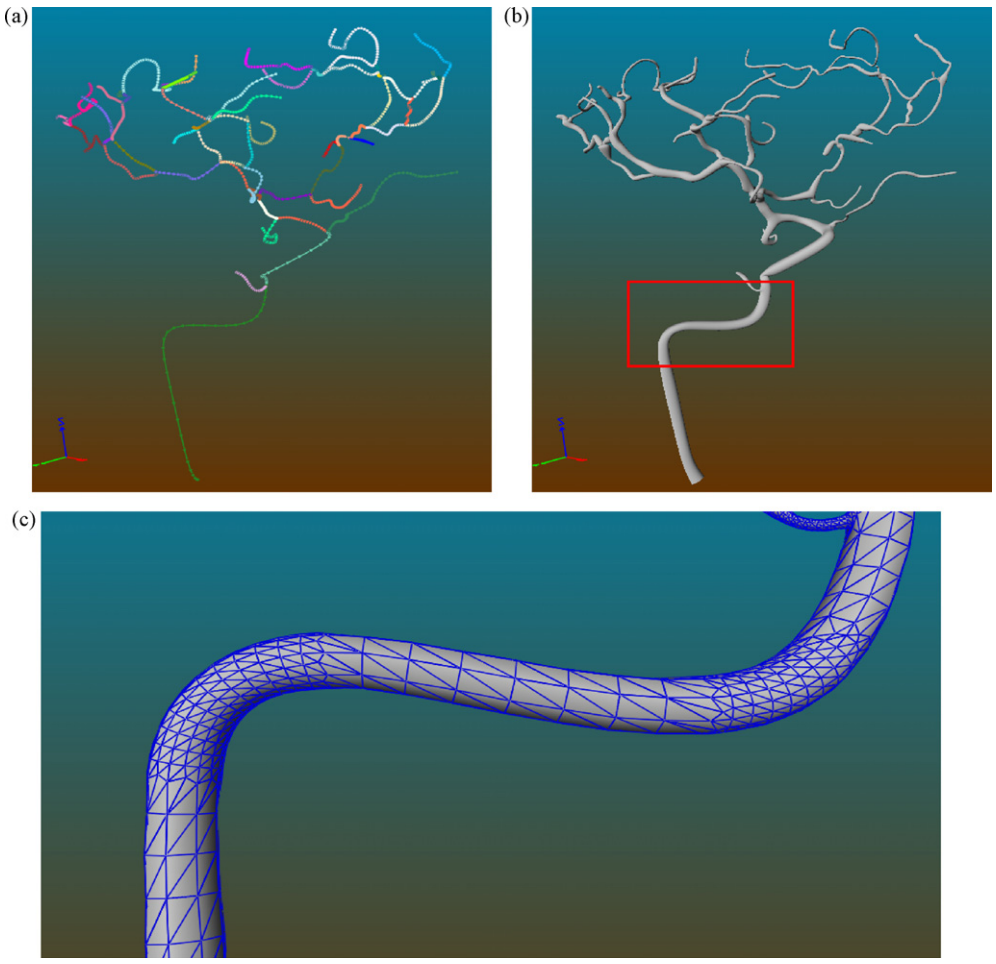

Fig. 7. (a) Bidirectional sampling result of a cerebral tree, (b) the generated surface using adaptive curvature-dependent subdivision, and (c) the zoom region of the red rectangle region in (b).

3. Results and discussion

We applied the proposed approach to visualize cerebral tree (Fig. 7), liver tree (Fig. 8 (left)) and aorta tree (Fig. 8 (right)). The generated surface offers a good balance between surface smoothness and surface size. A close check near branchings shows that transition at the branching is geometrically continuous and naturally smooth (Fig. 8). Fig. 7a shows a cerebral centerline tree, down-sampled by our bidirectional sampling strategy and processed with one level of curvature-dependent subdivision after one level of uniform subdivision. As shown in Fig. 7c, the regions with high curvature are approximated with more faces while those areas with relatively low curvatures are not. With our method, the reconstructed vessel surface can have fewer polygons while keeping comparable quality to that of the uniform subdivision.

3.1. Comparison between bidirectional sampling and unidirectional sampling

In the work of Felkel et al. [11,12], the centerline is down-sampled to a lower resolution such that the distance of the

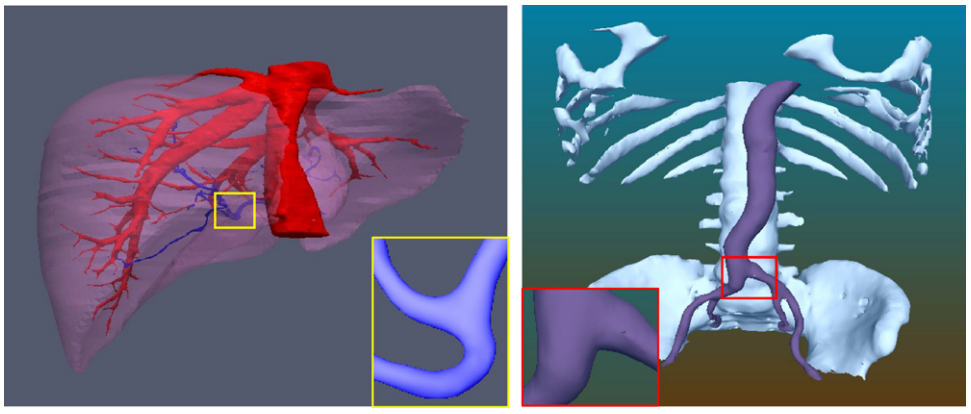

Fig. 8. Visualization of liver tree (left) and aorta tree (right) with our method.

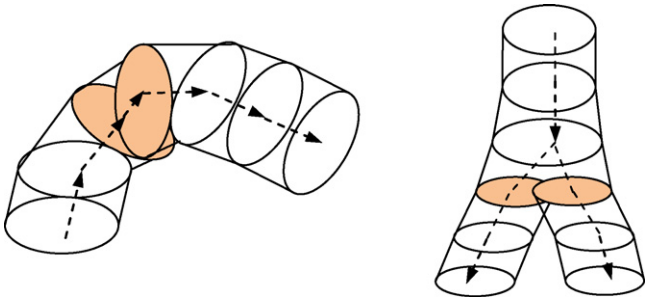

Fig. 9. For vessel segment with a large radius and curvature (left), or with small branching angle and large radius (right), the generated surface can be non-manifold.

neighboring segments is comparable to the vessel diameter. This technique is simple but neglects the significant change in curvature of the centerline which can yield non-manifold base mesh (Fig. 9). Furthermore, evenly sampling can not characterize the geometry of the vessel correctly. Therefore, Luboz et al. [19] used Eq. (1) to construct a non-linear equation and solved the equation by means of Broydn's method [26] to obtain new vertices. Unfortunately, this method may not get correct vertices, because the Broydn's method may not be convergent when a vertex in the centerline has a high curvature while its two adjacent vertices have a low curvature. Furthermore, solving the non-linear equation is time consuming especially when the input dataset is large.

Both [11] and [19] adopted unidirectional sample along the centerline, resulting in the first two (or the last two) vertices being too close (or far), as shown in Fig. 10a, and consequently the distance between the two vertices cannot meet the requirement of sampling. Therefore, the generated base mesh of this vessel segment can be very thin to make the transition at vessel joints coarse (Fig. 10c).

Our bidirectional sampling method can yield a better resolution (Fig. 10b) and guarantee that the distance between the first and last two segments is not too small (or large). Accordingly, the produced surface at branching is naturally smooth (Fig. 10d) without a flat twist (Fig. 10c) to avoid misinterpretation of vessel narrowing (false stenosis).

3.2. Determination of up-vectors

When a branch has multiple parents, Wu et al. [21] projected all the *up-vectors* of the parent branches onto the plane defined by the joint location and the normal of outgoing child segment, and then took the average of these projected *up-vectors* as the new *up-vector*. The drawback of this approach is that the produced *up-vector* may be singular [21]. When this happened, the *up-vector*

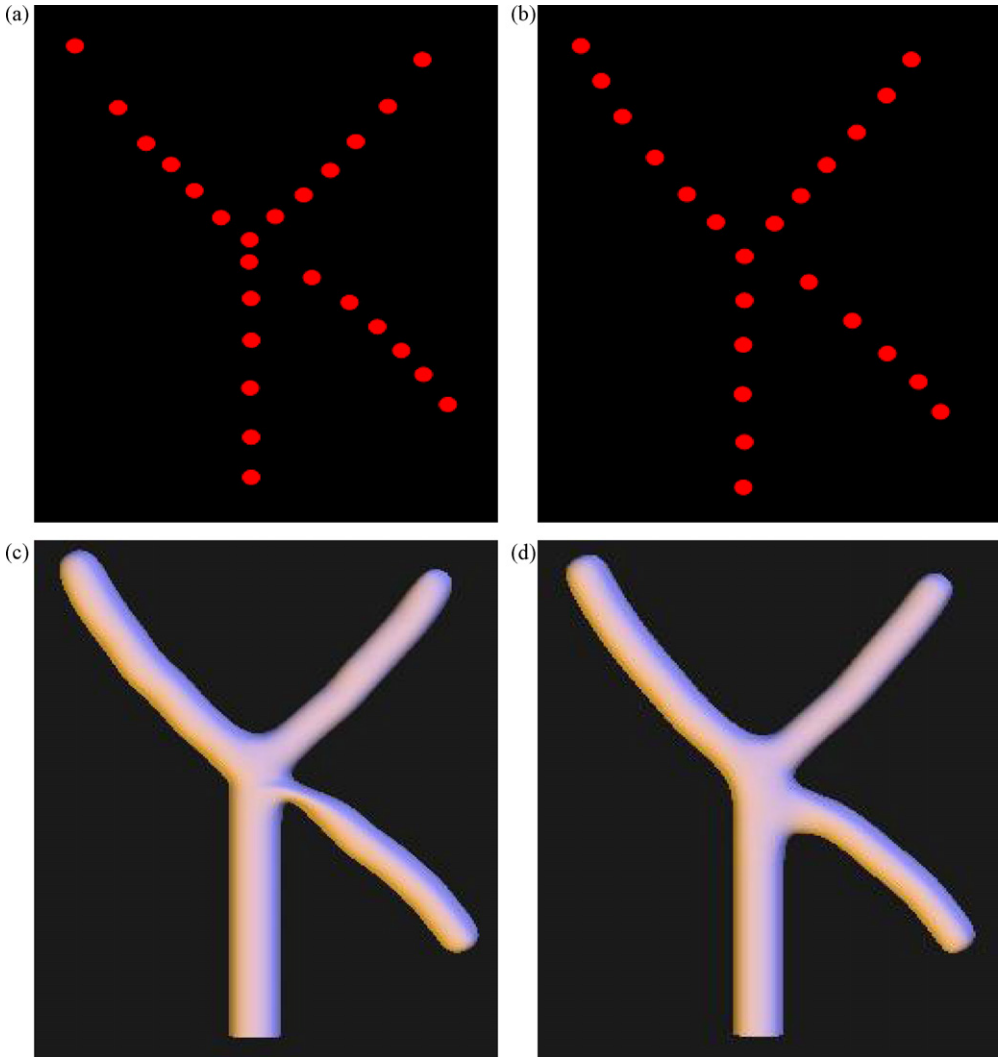

Fig. 10. Sampling centerline using unidirectional sampling (a), the proposed bidirectional sampling (b), generated surface based on unidirectional sampling (c), and generated surface from bidirectional sampling (d).

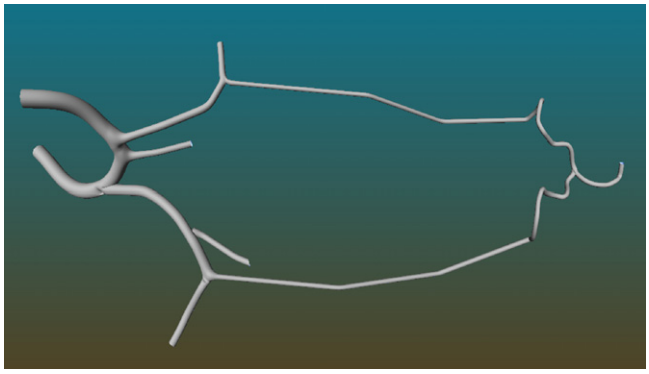

Fig. 11. Vessel segments with one loop and the enhanced visualization.

needs to be re-computed by choosing randomly a vector which is perpendicular to the first normal of the outgoing vessel segment. In our method, we only use the "positive" normals of all incoming parents to compute the normal at joint, and thus the computed normal will not be singular because the "negative" normals are not used for averaging (the normals whose included angle to the normal of incoming segment is larger than 90° are defined as negative, the remaining as positive [11,12]). Another advantage is that our method needs neither to compute the average of the *up-vectors* projected by each parent branch, nor to propagate the *up-vector* of other parent branch, instead, only the *up-vector* of the trunk parent branch needs to be calculated and propagated. The enhanced visualization by our proposed methods of vessel segments with one loop and multiple parents and children is given in Fig. 11.

3.3. Comparison of surface size

We now compare costs of uniform subdivision and adaptive subdivision in more detail. As mentioned previously, the numbers of polygons after one subdivision step is four times those of original polygons. Taking the cerebral tree for example once again, the initial mesh has 7834 triangles. A second level of uniform subdivision reaches 125,344 triangles as opposed to 86,450 triangles generated by our Gaussian curvature-dependent subdivision at the threshold θ (see below for explanation) of 0.95 which saves more than 30% in the size of derived surface. Continuing with uniform Loop refinement results in 501,376 triangles at the third level while 331,346 triangles produced by our adaptive method. The more the adaptive subdividing process is done, the more the reduction ratio in surface size will increase.

In our work, the adaptive process is controlled by a user-specific curvature threshold θ and only those regions whose curvature is larger than θ will be subdivided. If θ is zero, it means uniform subdivision, i.e. the whole model will be refined. In our experience, we found that θ between 0.90 and 0.95 can achieve a good trade-off between surface size and surface quality.

Table 1 shows the surface size produced by uniform subdivision, dihedral-based [25] and curvature-based adaptive subdivision. It can be seen that by using curvature-based refinement, there is always about 30–50% of saving in the surface size in comparison with those from the uniform subdivision scheme. For vessel tree with many highly curved branches, such as the cerebral tree, curvature-based adaptive subdivision outperforms dihedral angle-based subdivision in achieving trade-off between surface size and surface quality (see Section 3.4 for reason).

3.4. Comparison of surface quality

The smoothness of reconstructed surface can be measured by calculating the distribution of curvature on the surface. Here we compute Root Mean Square (RMS) curvature of both the minimal k_1 and the maximal k_2 principal curvatures of the produced surface respectively and RMS is defined by $\sqrt{(k_1^2+k_2^2)/2}$. It can be seen (Fig. 12) that the vessel surface quality is greatly improved by performing subdivision, and the surface produced by our adaptive subdivision (Fig. 12d), with a fewer approximation, has the same surface quality as the surface generated by the uniform subdivision. The reason for that is in subdivision surface, subdividing a flat surface (e.g. the region with RMS curvature being zero, as illustrated in Fig. 12) will not increase the smoothness of the surface but increase the size of the surface.

Table 1
Comparison of surface size produced by uniform subdivision, dihedral angle-based and curvature-based adaptive subdivision on three vascular structures (α and θ mean the threshold of dihedral angle and curvature respectively).

Data set	Polygon	Level	Uniform	Dihedral angle		Curvature	
			Polygon	Polygon	α	Polygon	θ
Cerebral tree	7834	1	31,336	31,024	120	22,346	0.90
		2	125,344	108,952	144	86,450	0.95
		3	501,376	309,230	160	248,826	0.925
Liver tree (in blue)	2256	1	9024	6968	140	6112	0.90
		2	360,96	20,384	155	19,598	0.93
Aorta tree	1845	1	7380	5078	160	4772	0.90
		2	29,520	18,545	170	19,644	0.95

We also use *radii-radio* measure to evaluate the triangle quality of a given surface. The measure is defined as $\rho = R/r$ (R and r are the circumscribed and the inscribed circles of a given triangle respectively) [27]. It is found that the quality of triangles of our method is the same as those produced by the uniform subdivision, except for those triangles which are to be subdivided at the next level, but whose neighbors are not, since these triangles are always degenerated. Unfortunately, in adaptive refinement these triangles can not be avoided because they are created to remove cracks. Therefore, it is better to further optimize these triangles by the way like edge-swap since these triangles may cause numerical problem if the produced surface is used for computational fluid dynamics simulations.

We also compare curvature-dependent subdivision to dihedral angle-based subdivision [25]. The comparison demonstrates that curvature-based measure can more accurately characterize the geometry of vessel surface than angle-based measure, as shown in Fig. 12. The reason is that dihedral angle method, which uses the angles between normals of a triangle with adjoining triangle normals, is a simple measure to identify which regions of surface are flat, but not a good measure for identifying highly curved regions. Another disadvantage of dihedral scheme is that it can not be applied in succession for a surface, as pointed out in [25].

3.5. Analysis of complexity and efficiency

Let n be the number of processed segments and S be the number of the input sections, namely the sum of sections of the individual input segments. The complexity of the proposed bidirectional sampling process is $O(S)$. Since n is generally much less than S, the complexity of generating base quadrilateral mesh process is $O(S+n) = O(S)$. The maximum number of the generated quadrilaterals is $4S$ and the number of vertices is $4S+4$, thus the complexities of triangulation process and curvature estimation process are $O(4S)$ and $O(4S+4)$ respectively. After triangulation, the number of triangles is $8S$ and therefore the complexity of our adaptive subdivision process is less than $O(8S)$, while the uniform subdivision is $O(8S)$.

Table 2 shows the timing performance of constructing uniform and adaptive subdivision surfaces from several vascular centerline trees. The algorithm is implemented in Visual C++ 2005 and tested on Pentium D processor at 2.80 GHz with a 3.00 GB memory.

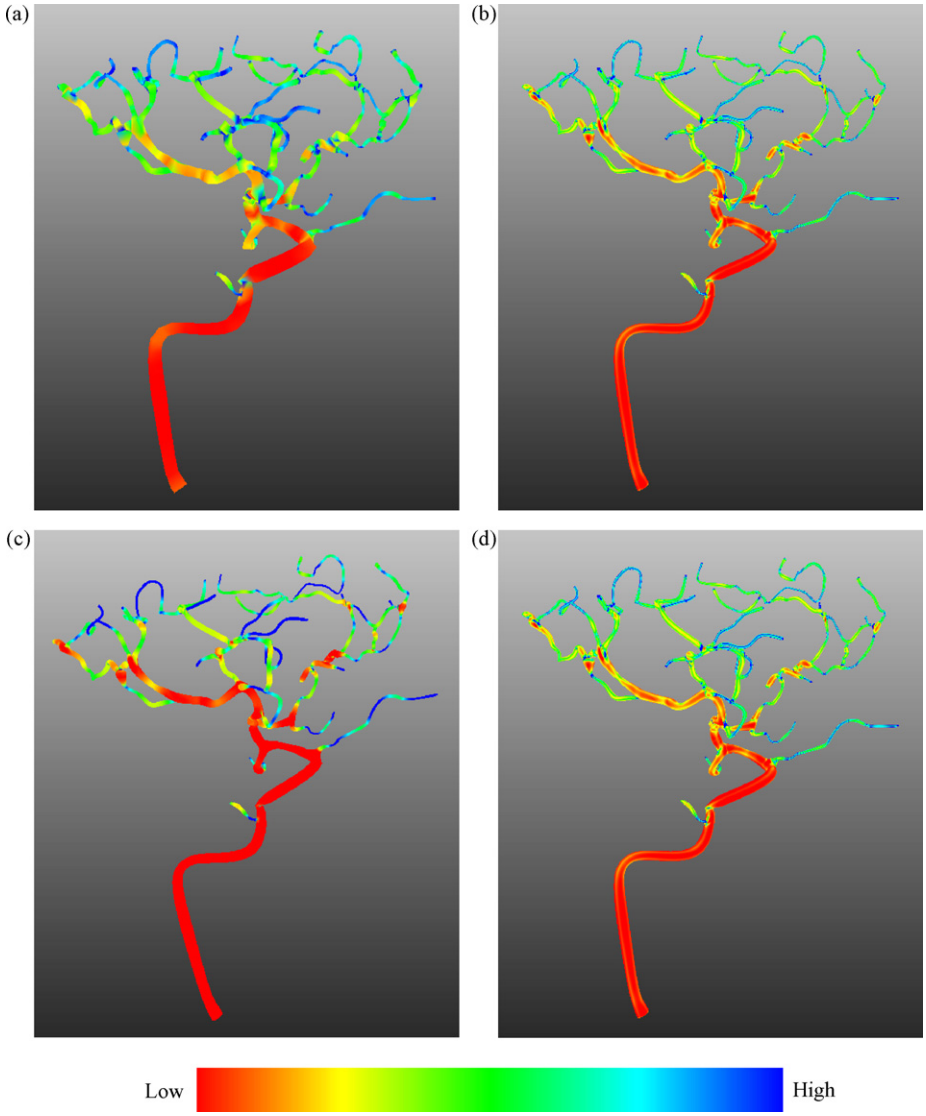

Fig. 12. Color-coded visualization of RMS curvature distribution for the vessel surface. (a) The initial surface, (b) the result of two levels of uniform subdivision on the initial surface, (c) the result of two levels of adaptive subdivision based on dihedral angle with threshold 165° on the initial surface, and (d) the result of two levels of adaptive subdivision based on Gaussian curvature with threshold 0.95 on the initial surface.

Table 2
Timing performance for each process of generating subdivision surface on three vascular trees.

Data set	Data size		Method	Run time (s)			
	n	*S*		Sam	MeGen	TriEst	Sub
Cerebral tree	61	1523	Uni	0.001	4.425	–	0.397
			Ang	0.001	4.367	0.030	0.309
			Cur	0.001	4.367	0.115	0.306
Liver tree	131	3107	Uni	0.003	7.875	–	1.186
			Ang	0.003	7.545	0.109	1.034
			Cur	0.003	7.545	0.324	1.029
Phantom tree	52	2832	Uni	0.002	6.717	–	0.787
			Ang	0.002	6.538	0.093	0.640
			Cur	0.002	6.538	0.279	0.636

Uni: one level of uniform subdivision; Ang: one level of subdivision based on dihedral angle with threshold 165°; Cur: one level of subdivision based on based on Gaussian curvature with threshold 0.90; Sam: unidirectional sampling for Uni and bidirectional sampling for Ada; MeGen: base quadrilateral mesh generating process; TriEst: for Ang, TriEst means triangulation and dihedral angle estimation process; for Cur, TriEst means triangulation and curvature estimation process; Sub: subdivision process.

It is clearly seen that the most time-consuming process is generating the base quadrilateral mesh because the process is a recursive procedure whose complexity depends on the input vascular tree structure. Compared to the uniform subdivision-based method [11,19], our method needs additional processes of triangulation and curvature estimation; fortunately, these two processes need a little time and help to achieve curvature-dependent adaptive subdivision which saves a great deal of memory complexities (discussed in Section 3.3). In contrast to dihedral angle-based subdivision, our method is a bit slower as the curvature estimation is a bit more complicated than dihedral angle computation.

4. Conclusion

In this paper, we have presented a method for visualizing vascular structures defined by its centerline and radius. To achieve a smooth transition at branches, we proposed a bidirectional sampling strategy; by means of that, the centerline can be downsampled to generate a topologically-correct base mesh. To deal with complex topology of vascular structures, we devised a way to determinate normals and *up-vector* at joint branchings. Finally,

to reach a better trade-off between the surface quality and the surface size, we exploited the differential geometric property of a given surface and used curvature-dependent subdivision to generate the surface for visualization. Experimental tests on a variety of vascular structures demonstrate our method can achieve a high-quality surface visualization with fewer polygons in the approximation while keeping the same smoothness as the uniform subdivision. Our method can not only reduce the size of resulted surface in storage space but reduce the computational load especially at higher levels of subdivision, thus the speed of rendering and interaction can be drastically improved. In the future, we will develop more interactive facilities (e.g. annotation and angle qualification) for geometric analysis [28] of vascular structures, and for exploring vasculature in our interventional neuroradiology simulator system which aims to provide a virtual environment for physicians to learn and practice without putting patients at risk [29].

Acknowledgements

The authors thank all the anonymous reviewers for their valuable suggestions and comments, and thank Xiaohua Du for his manual segmentation of the intrahepatic vasculature (Fig. 8 (left)). This work was supported by National Natural Science Foundation of China under Grant No. 60803108 and China Postdoctoral Science Foundation (Grant No. 20100470560).

References

[1] Oeltze S, Preim B. 3D visualization of vasculature: an overview. In: Visualization in medicine and life sciences. Springer; 2007. p. 19–39.
[2] Volkau I, Ng TT, Marchenko Y, Nowinski WL. On geometric modeling of the human intracranial venous system. IEEE Trans Med Imag 2008;27(6):745–51.
[3] Bühler K, Felkel P, Cruz AL. Geometric methods for vessel visualization and quantification – a survey. In: Brunnet G, Hamann B, Müller H, editors. Geometric modeling for scientific visualization. 2004. p. 399–420.
[4] Gülsün MA, Tek H. Geometric modeling of tubular structures. In: IEEE computer society conference on computer vision and pattern recognition workshops (CVPRW). 2008. p. 1–8.
[5] Masutani Y, Masamune K, Dohi T. Region-growing-based feature extraction algorithm for tree-like objects. In: Proceedings of visualization in biomedical computing. 1996. p. 161–71.
[6] Hahn HK, Preim B, Selle D, Peitgen HO. Visualization and interaction techniques for the exploration of vascular structures. In: IEEE visualization 01. 2001. p. 395–402.
[7] Höhne KH, Pflesser B, Pommert A, Riemer M, Schubert R, Schiemann T, et al. A realistic model of the inner organs from the visible human data. In: Proceedings of the international conference on medical image computing and computer-assisted intervention (MICCAI). 2000. p. 776–85.
[8] Bornik A, Reitinger B, Beichel R. Reconstruction and representation of tubular structures using simplex meshes. In: Proceedings of winter school of computer graphics (WSCG). 2005. p. 61–5.
[9] Oeltze S, Preim B. Visualization of vascular structures with convolution surfaces. In: Proceedings of IEEE/Eurographics symposium on visualization (VisSym). 2004. p. 311–20.
[10] Oeltze S, Preim B. Visualization of vascular structures with convolution surfaces: method, validation and evaluation. IEEE Trans Med Imag 2005;25(4):540–9.
[11] Felkel P, Wegenkittl R, Bühler K. Surface models of tube trees. In: Proceedings of the computer graphics international (CGI). 2004. p. 70–7.
[12] Felkel P, Kanitsar A, Fuhrmann AL, Wegenkittl R. SMART-surface models from by axis-and-radius-defined tubes. TR-VRVis-2002-008. Vienna, Austria: VRVis Research Center; 2002.
[13] Lorensen WE, Cline HE. Marching cubes: a high resolution 3D surface construction algorithm. In: Proceedings of ACM SIGGRAPH. 1987. p. 163–9.
[14] Schumann C, Neugebauer M, Bade R, Preim B, Peitgen HO. Implicit vessel surface reconstruction for visualization and simulation. Int J CAS 2008;2(5):275–86.
[15] Schumann C, Oeltze S, Bade R, Preim B, Peitgen HO. Model-free surface visualization of vascular trees. In: Eurographics/IEEE-VGTC symposium on visualization. 2007. p. 283–90.
[16] Ohtake Y, Belyaev A, Alexa M, Turk G, Seidel HP. Multilevel partition of unity implicits. ACM Trans Graph 2003;22:463–70.
[17] Klein J, Bartz D, Friman O, Hadwiger M, Preim B, Ritter F, et al. Advanced algorithms in medical computer graphics. In: Proceedings of Eurographics 2008. 2008. p. 25–44.
[18] Zorin D, Schroder P. Subdivision for modeling and animation. SIGGRAPH 2000 course notes; 2000. p. 13–16.
[19] Luboz V, Wu X, Krissian K, Westin CF, Kikinis R, Cotin S, et al. A segmentation and reconstruction technique for 3d vascular structures. In: Proceedings of the international conference on medical image computing and computer-assisted intervention (MICCAI). 2005. p. 43–50.
[20] Calabi E, Olver PJ, Shakiban C, Tannenbaun A, Haker S. Differential and numerically invariant signature curves applied to object recognition. Int J Comput Vision 1998;26(2):107–35.
[21] Wu X, Luboz V, Krissian K. Smooth vasculature reconstruction from patient scan. In: Proceedings of the virtual reality interactions and physical simulation, VRIPHYS poster. 2005.
[22] Gatzke T, Grimm C. Improved curvature estimation on triangular meshes. In: Eurographics symposium on geometry processing. 2003. p. 57–67.
[23] Li SZ. Adaptive sampling and mesh generation. Comput Aided Design 1995;27(3):235–40.
[24] Karkanis T, Stewar AJ. Curvature-dependent triangulation of implicit surfaces. IEEE Comput Graph 2001;21(2):60–9.
[25] Amresh A, Farin G, Razdan A. Adaptive subdivision schemes for triangular meshes. In: Farin G, Hagen H, Hamann B, editors. Hierarchical and geometric methods in scientific visualization. Springer-Verlag; 2003. p. 319–27.
[26] Numerical recipes in C. Cambridge; 1992.
[27] Pebay PP, Baker TJ. A comparison of triangle quality measures. In: 10th international meshing roundtable. 2001. p. 327–40.
[28] Piccinelli M, Veneziani A, Steinman DA, Remuzzi A, Antiga L. A framework for geometric analysis of vascular structures: application to cerebral aneurysms. IEEE Trans Med Imag 2009;28(8):1141–55.
[29] Ma X. Latest development of an interventional radiology training simulation system: NeuroCath. In: 12th international conference on human-computer interaction, vol. 4561. 2007. p. 684–93.

Jianhuang Wu received his Ph.D. degree from Shenyang Institute of Automation, Chinese Academy of Sciences in 2007. He is currently an assistant professor at the Center for Human-Computer Interaction, Shenzhen Institutes of Advanced Technology, Chinese Academy of Sciences. His research interests include medical visualization, virtual surgery and computer graphics. He now is a PI of research project funded by the National Natural Science Foundation of China.

Renhui Ma is now a M.S. student at the Center for Human-Computer Interaction, Shenzhen Institutes of Advanced Technology, Chinese Academy of Sciences. His research interests are geometric modeling and computer graphics.

Xin Ma received his M.S. degree from National University of Singapore in 2002. He is now an associate professor at the Center for Human-Computer Interaction, Shenzhen Institutes of Advanced Technology, Chinese Academy of Sciences. From 2000 to 2007, he served as senior associate scientist in Biomedical Imaging Lab, Agency of Science, Technology and Research of Singapore. After that he joined Shenzhen Institutes of Advanced Technology. He has published more than 30 papers, filed more than 5 international inventive patents. His research interests include virtual surgery and computer assisted surgery.

Fucang Jia received his Ph.D. degree in Computer Application Technology from Institute of Computing Technology, Chinese Academy of Sciences in 2004. He is currently an associate professor at the Center for Human-Computer Interaction, Shenzhen Institutes of Advanced Technology, Chinese Academy of Sciences. From August 2004 to April 2008, he engaged in R&D and management in Neurosurgery planning and navigation, Orthopedic surgery navigation, medical image storage and transmission system in Shenzhen Anke High-tech Co., Ltd. From December 2005 to August 2007, He was a postdoctoral research fellow in Zhejiang University and Anke High-tech Co., Ltd. He has published more than 40 papers. Presently, he focuses his research on surgical plan navigation and medical imaging information system.

Qingmao Hu received his Ph.D. degree from Huazhong University of Science and Technology in 1990. He is now a professor and associate director of the Center for Human-Computer Interaction, Shenzhen Institutes of Advanced Technology, Chinese Academy of Sciences. He served as lecturer, associate professor, and professor in the First Military Medical University from 1990 to 1996, and guest scientist and post doctor in University of Bern, Switzerland from1996 to 2000. From 2000 to 2007, he served as associate member, member and senior scientist in Biomedical Imaging Lab, Agency of Science, Technology and Research of Singapore. After that he joined Shenzhen Institutes of Advanced Technology, and was awarded the Hundred Talent Program, Chinese Academy of Sciences in 2008. He has published more than 100 papers, filed more than 20 international inventive patents, and won RSNA merit awards 3 times, ASNR 1st prize 1 time. His research areas are: image analysis, medical image processing, computer-aided diagnoses and therapy, computer vision, and pattern recognition.